Hindawi
Shock and Vibration
Volume 2020, Article ID 8901794, 10 pages
https://doi.org/10.1155/2020/8901794

Research Article

Peak-Based Mode Decomposition for Weak Fault Feature Enhancement and Detection of Rolling Element Bearing

Zhi Xu,[1,2,3] **Gang Tang**,[2] **and Mengfu He**[1]

[1]*State Key Laboratory of Nuclear Power Safety Monitoring Technology and Equipment, Shenzhen, Guangdong 518172, China*
[2]*College of Mechanical and Electrical Engineering, Beijing University of Chemical Technology, Beijing 100029, China*
[3]*Aviation Key Laboratory of Science and Technology on Fault Diagnosis and Health Management, Shanghai Aero Measurement & Control Technology Research Institute, Shanghai 201601, China*

Correspondence should be addressed to Gang Tang; tanggang@mail.buct.edu.cn

Received 16 September 2019; Revised 4 January 2020; Accepted 17 January 2020; Published 9 April 2020

Academic Editor: Felix Albu

Rolling element bearings are widely used in rotating machinery to support shafts, whose failures may affect the health of the whole system. However, strong noise interferences often make the bearing fault features submerged and difficult to be identified. Peak-based wavelet method is such a way to reduce certain noise and enhance the fault features by increasing the sparsity of monitored signals. But peak-based wavelet parameters need to be optimized due to the determined basis function and constant resolution, which will affect the efficiency of vibration signal analysis. To address these problems, a peak-based mode decomposition is proposed for weak bearing fault feature enhancement and detection. Firstly, to enhance the differences between repetitive transients and high-frequency noise, a peak-based piecewise recombination is used to convert the middle frequency parts into low-frequency ones. Then, the recombined signal is processed by empirical mode decomposition, combining with a criterion of cross-correlation coefficients and kurtosis. Subsequently, a backward peak transformation is performed to obtain the enhanced signal. Finally, the fault diagnosis is implemented by the squared envelope spectrum, whose normalized squared magnitude is used as a bearing fault indicator. The analysis results of the simulated signals and the experimental signals show that the proposed method can enhance and identify the weak repetitive transient features. The superiority of the proposed method for faint repetitive transient detection is also verified by comparing with the peak-based wavelet method.

1. Introduction

Rolling element bearing (REB) is one of the most widely used elements in rotating machinery and sudden bearing failures may cause system outage [1]. Statistics show that faulty bearings contribute to about 30% of the failures in rotating machinery [2, 3]. Thus the bearing fault diagnosis is of great significance for ensuring a safe and stable operation of rotating machinery.

In pursuit of an effective bearing fault diagnosis, a series of methods have been developed in recent decades, e.g., vibration monitoring, acoustic emission monitoring, temperature monitoring, and oil monitoring [4, 5]. Vibration-based techniques are very attractive because of its noninvasive way and high sensibility to weak faults. In general, when a REB fails, the vibration amplitude intensity will increase significantly. At this point, the abnormal state can be alarmed by parameters in the time domain such as root mean square, kurtosis, and skewness. However, time-domain processing methods are not always effective in fault identification, especially when the fault features are very weak submerged with strong noise interferences.

Frequency domain analysis is a commonly used alternative way, in which domain, the fault characteristic frequencies are often more obviously relevant to the source of bearing fault. But there often exists some slippage in REB motions, which results in uncertainty in the interarrival instant of the impacts [6, 7]. The randomness resulting from jitter in the impact, despite the magnitude of a few percent of the fault period, changes the entire statistical structure of the

signal [8, 9]. Therefore, spectrum analysis is not always effective in all cases, especially for weak repetitive transients.

Envelope demodulation can help to solve the serious slippage problem in the frequency domain, which is recognized as a powerful bearing diagnosis technique and popularly used [10, 11]. However, the excited vibration signal of a fault component is passed to the sensor through a complex transmission path, in which the interference noise will be introduced inevitably. Then, the impact of the fault-related signal will be suppressed, which weakens the effectiveness of the envelope analysis [12, 13].

Wavelet transform is helpful to reduce the influence of background noise due to its flexile time-frequency resolutions [14, 15]. Kumar and Singh [16] proposed wavelet-based methods for feature extraction, in which the fault-related wavelet coefficients are selected with thresholding rules. Mishra et al. [17] proposed a sigmoid function-based wavelet thresholding for signal denoising. Du et al. [18] proposed a hybrid method which combines the Morlet wavelet filter and sparse code shrinkage for bearing fault diagnosis. These methods optimize the wavelet parameters and try to reduce the influence of background noise, which can improve the effectiveness of envelope analysis. Yet, these wavelet-based methods essentially improve the sparsity differences between noise and fault signal through linear variations, and there is still plenty of room for improvement. Wang et al. [19] improves the signal sparsity by the nonlinear peak-based wavelet transform, and fault features can be enhanced obviously and detected easily. However, there are many parameters that need to be optimized in the wavelet transform, such as wavelet basis function and thresholding values.

In order to compensate for the insufficient adaptability of the peak-based wavelet transform, a new mode decomposition method, based on empirical mode decomposition (EMD), is proposed for enhancing and detecting the bearing fault feature in this paper. EMD is an adaptive signal decomposition method that transforms a signal into several intrinsic mode functions (IMFs) [20]. In the proposed method, a peak-based piecewise recombination (PPR) is firstly used to enhance the differences between repetitive transients and high-frequency noise. Subsequently, the correlation coefficients and kurtosis criteria are used to select the IMFs, which is decomposed by EMD from the recombined signal. Then, the enhanced signal is obtained by a backward peak transform. Finally, the normalized squared-magnitude of the squared envelope spectrum is used as a bearing fault indicator. The peak-based mode decomposition overcomes the difficulties of parameter selections, and it is adaptive to the analysed signal, thus can be easily implemented in practice. Case studies with simulation and experiments show that the proposed method can enhance the weak bearing fault signals more effectively.

The remainder of this paper is organized as follows. In Section 2, the basic theory of the PPR and EMD is introduced. Then, the proposed method is presented. Numerical simulation is performed in Section 3. Experiments and comparisons are presented in Section 4. Finally, conclusions are presented in Section 5.

2. Methods

2.1. Peak-Based Piecewise Recombination. Peak-based piecewise recombination (PPR), or so-called peak transformation (PT), is a nonlinear geometric transformation method which enhances the differences between repetitive transients and high-frequency noise [21]. A brief description of PT is given as follows.

Definition 1.

(a) Cascade of Curve Segments. Given two curve segments $f_1(x)$ and $f_2(x)$ defined over finite intervals $[a_1, b_1]$ and $[a_2, b_2]$ with $b_1 \le a_2$—the cascade of these two curve segments yields a new curve segment $f(x)$, defined as

$$f(x) = \begin{cases} f_1(x), & x \in [a_1, b_1], \\ f_2(x) - f_2(a_2) + f_1(b_1), & x \in (b_1, b_1 + b_2 - a_2] \end{cases} \tag{1}$$

We denote this cascading operation by

$$f(x) = f_1(x) \oplus f_2(x). \tag{2}$$

(b) n-Point Forward Peak Transform. A continuous function $f(x)$ is defined over $[a, b]$. This interval is partitioned into $n+1$ subintervals by n points $a < x_1 < x_2 < \cdots x_n < b$, with $x_0 = a$ and $x_{n+1} = b$. The forward transformation of n points based on piecewise recombination of peaks can be defined as

$$PT[f(x)] = g_o(x) \oplus g_e(x), \tag{3}$$

where

$$\begin{aligned} g_o(x) &= f_1(x) \oplus f_3(x) \oplus \cdots \oplus f_{2\lfloor (n-1)/2 \rfloor + 1}(x), \\ g_e(x) &= f_2(x) \oplus f_4(x) \oplus \cdots \oplus f_{2\lfloor n/2 \rfloor}(x), \end{aligned} \tag{4}$$

which denotes the cascades of all odd- and even-numbered curve segments, respectively. Here, $2(n-1)/2 + 1$ and $2n/2$ are, respectively, the largest odd and even integers that are less than or equal to n. In forward PT, we first cascade all odd-numbered curve segments then all even-numbered curve segments and recompose a new curve. Figure 1 shows an example of five-point PT. It can be seen that the reversible recombination only changes the order of the piecewise curves. A detailed algorithm of the PT can be found in [21].

2.2. Empirical Mode Decomposition. Empirical mode decomposition (EMD) is an adaptive signal decomposition method that transforms a signal into several intrinsic mode functions (IMFs) [20, 22], and IMFs must meet the following requirements:

(1) The maximum difference between the number of extremum points and the number of zeros is one.

(2) The upper and lower envelopes are locally symmetric.

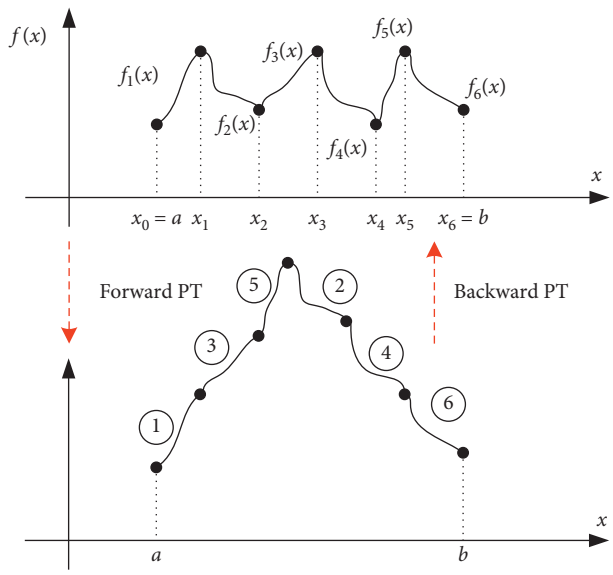

Figure 1: Example of a five-point PT.

For a given signal $f(x)$, the effective algorithm of EMD can be described as follows:

(1) Identify all extrema of $f(x)$.

(2) Interpolate between minima (resp. maxima), ending up with some "envelope" $l(x)$ (resp., $u(x)$).

(3) Compute the average $m(x) = (l(x) + u(x))/2$.

(4) Extract the detail $d(x) = f(x) - m(x)$.

(5) Iterate on the residual $d(x)$.

From the above steps, the signal can be decomposed into a sum of several "mode" and residual components:

$$f(x) = m_K(x) + \sum_{k=1}^{K} d_k(x), \tag{5}$$

where $m_K(x)$ stands for a residual "trend" and $\sum_{k=1}^{K} d_k(x)$, $k = 1, \ldots, K$ stands for a series of IMFs.

2.3. Enhancement Frame with Peak-Based Mode Decomposition. Due to the problems of interpolation error, boundary effect, and overdecomposition, pseudocomponents are often existing in IMFs. In other words, there may exist some components which are unrelated to the original signal. The frequency components contained in these pseudocomponents may overlap with the bearing fault characteristic frequency bands. Therefore, these pseudocomponents should be removed for bearing fault features detection.

Kurtosis and correlation coefficient are commonly used to estimate these pseudocomponents.

Kurtosis is a dimensionless parameter to represent a signal, which is defined as

$$Ku = \frac{E(x-\mu)^4}{\sigma^4}. \tag{6}$$

In the formula, μ and σ are the mean and standard deviation of signal x, respectively, and $E(t)$ represents the expected value of variable t.

Correlation coefficient represents the correlation between each IMF and the original signal, which is defined as

$$\rho_{x,\mathrm{IMF}_k} = \frac{\max\left(R_{x,\mathrm{IMF}_k}(\tau)\right)}{\max\left(R_x(\tau)\right)}. \tag{7}$$

The present paper proposed an enhancement frame for vibration signals combining peak-based mode decomposition and envelope demodulation. The steps are summarized as follows:

(1) Peak-based piecewise recombination of a vibration signal: the vibration signal $f(x)$, according to equation (3), is transformed into a recombined signal $R(x)$ by piecewise recombination.

(2) EMD decomposition of the recombined signal $R(x)$: the recombined signal $R(x)$ is decomposed into several IMFs through EMD:

$$R(x) = r_K(x) + \sum_{k=1}^{K} \mathrm{IMF}_k(x). \tag{8}$$

(3) Pseudocomponent removal: the pseudocomponents are determined by kurtosis and correlation coefficient. The effective signal $e(x)$ is obtained by superimposing the IMF after removing the pseudocomponents.

(4) Backward peak transform: put the effective signal segments $e(x)$ to their original positions, and a denoised signal $f'(x)$ is generated.

(5) Standardized squared envelope spectrum (SSES): conventionally, the squared envelope spectrum (SES) is defined as

$$\mathrm{SES}(f'(x)) = \left|DT\, DT\left\{E(x)^2\right\}\right|, \tag{9}$$

where

$$\begin{aligned} E(x) &= \sqrt{[f'(x)]^2 + [H(f'(x))]^2}, \\ H(f'(x)) &= \frac{1}{\pi}\int_{-\infty}^{+\infty} \frac{f'(\tau)}{x-\tau}\,\mathrm{d}\tau. \end{aligned} \tag{10}$$

Processing the signal by different methods will result in different magnitude of squared envelope spectrum. But a bearing fault is often detected by a relative value of the characteristic frequency of the fault, so the signals are standardized that the results of different methods can be compared. Therefore, the standardized squared envelope spectrum (SSES) is defined as

$$A_{\mathrm{SSES}}(f'(x)) = \frac{A_{\mathrm{SES}}(f'(x)) - \mu(A_{\mathrm{SES}}(f'(x)))}{\sigma(A_{\mathrm{SES}}(f'(x)))}, \tag{11}$$

where $A_{\mathrm{SES}}(f'(x))$ is the amplitude of $\mathrm{SES}(f'(x))$.

(6) Fault characteristic frequency extraction: the envelope spectrum is obtained by Fourier analysis, and different types of rolling bearings are distinguished.

In brief, these steps are shown in Figure 2.

3. Numerical Simulation

In order to verify the reliability of the proposed method in this paper, a fault model [23] was used to simulate the impact signal generated by an inner ring fault and a strong noise was added to simulate the early bearing fault signal of the inner ring mixed with noise interferences.

$$\begin{cases} x(t) = s(t) + n(t) = \sum_i A_i h(t - iT - \tau_i) + n(t), \\ h(t) = \exp(-Ct)\sin(2\pi f_n t), \\ A_i = A_0 \sin(2\pi f_r t). \end{cases} \tag{12}$$

In the simulation, $s(t)$ denotes the periodic impact component, the amplitude A_0 is 0.5, the rotation frequency f_r is 20 Hz, the attenuation coefficient C is 800, the resonance frequency f_n is 4000 Hz, and the ball pass frequency of inner race ($f_i = 1/T$) is 110 Hz. The small fluctuation τ_i of the i-th shock relative to the period T obeys the normal distribution of zero-mean, and the standard deviation is 0.5% of the frequency of rotation. $n(t)$ is the Gaussian white noise component, and the signal-to-noise ratio of the noise signal is −12 dB. The sampling frequency f_s is 12000 Hz, and the points of signal are 8192.

Waveform and spectrum of the simulated signal are shown in Figure 3. Comparing Figures 3(a) and 3(b), it can be found that the periodic pulse in the simulation signal is completely submerged by noise and there is no regularity. Figure 3(d) is the envelope spectrum of the simulation signal, and there is no prominent frequency.

Analysis results of the simulated signal by the proposed method are shown in Figure 4(a). Compared with Figure 3(b), the impact component in the signal is significantly increased. Envelope analysis is performed as shown in Figure 4(b). The amplitude of the spectrum at the ball pass frequency of the inner race and its multiple harmonics become obvious and the characteristic frequency information is accurately extracted.

4. Experiments and Comparisons

4.1. Experiments. In order to verify the effectiveness of peak-based mode decomposition, the vibration tests of the REB are performed. The test bench is shown in Figure 5.

In the experiments, electron-discharge machining was adopted to introduce single-point defects on the inner raceway, outer raceway, and rolling element of different bearings, with fault widths of 3 mm, 7 mm, and 7 mm, respectively, and depths of 5 mm, 25 mm, and 25 mm. The vibration signals are measured by an accelerometer, located at the top of the bearing box (CH1, as shown in Figure 5).

REB components have their specific fault characteristic frequencies, such as the ball pass frequency of the outer race (BPFO), the ball pass frequency of the inner race (BPFI), the ball spin frequency(BSF), and the cage frequency(CF). Their respective calculation formulas are as follows:

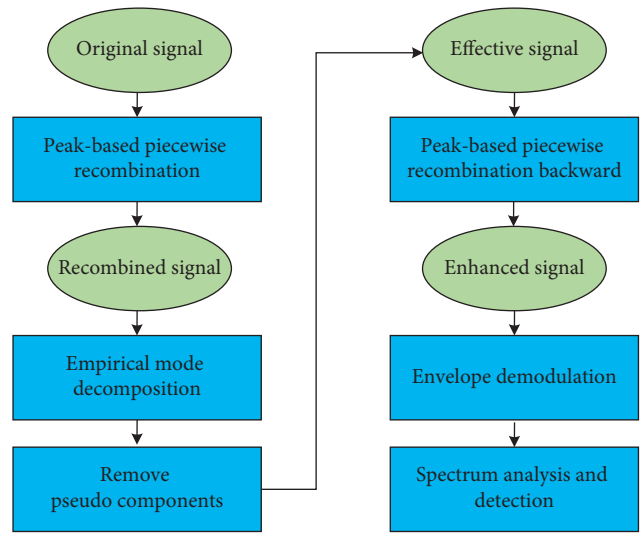

Figure 2: Flowchart of the proposed enhancement scheme for the weak fault signal.

$$\text{BPFO} = \frac{Z\omega}{2}\left(1 - \frac{d}{D}\cos\alpha\right), \tag{13}$$

$$\text{BPFI} = \frac{Z\omega}{2}\left(1 + \frac{d}{D}\cos\alpha\right), \tag{14}$$

$$\text{BSF} = \frac{D\omega}{2d}\left(1 - \left(\frac{d}{D}\cos\alpha\right)^2\right), \tag{15}$$

$$\text{CF} = \frac{1}{2}\left(1 - \frac{d}{D}\cos\alpha\right), \tag{16}$$

where Z is the number of rolling elements in the REB, ω is the shaft rotation frequency in rad/s, d is the diameter of rolling element, D is the diameter of the REB, and α is the contact angle.

According to equations (13)–(16), the theoretical fault characteristic frequencies of different rolling bearing parts are calculated, as listed in Table 1.

Four common conditions were studied, including a perfectly healthy bearing, a bearing with point defect on the outer race, a bearing with point defect on the inner race, and a bearing with point defect on the rolling element. In all experiments, the sampling frequency was 100 kHz and the rotating speed was 1300 rpm. The time-domain waveforms of REB vibration signals are shown in Figure 6.

In order to investigate the differences between vibration signals of different fault types, envelope demodulation is used for the signals of three typical bearing faults, such as the outer race fault, inner race fault, and rolling element fault. The results are shown in Figure 7. In Figure 7(a), the shaft rotation frequency (SRF) is higher than other frequencies, which shows that the test bench is slightly unbalanced. In Figure 7(b), the magnitude of BPFO is lower than the second

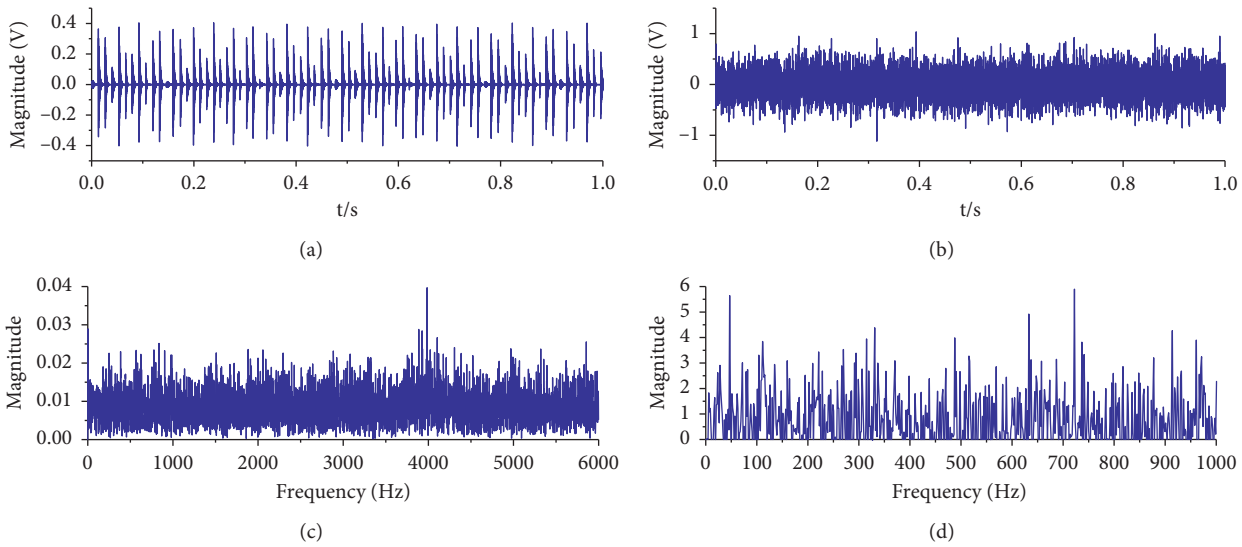

Figure 3: Waveform, spectrum, and envelope spectrum of the simulated signal. (a) Waveform of the impact signal. (b) Waveform of the simulated signal. (c) Spectrum of the simulated signal. (d) Envelope spectrum of the simulated signal.

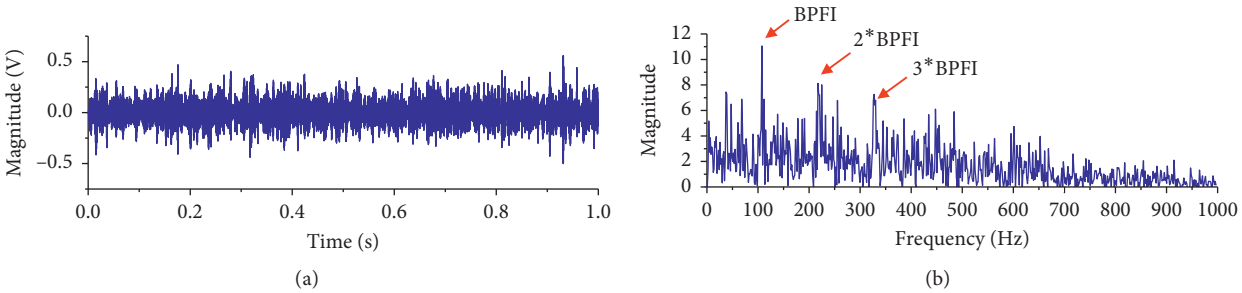

Figure 4: Analysis results of the simulated signal by the proposed method. (a) The result of the peak-based mode decomposition. (b) Envelope spectrum of the result.

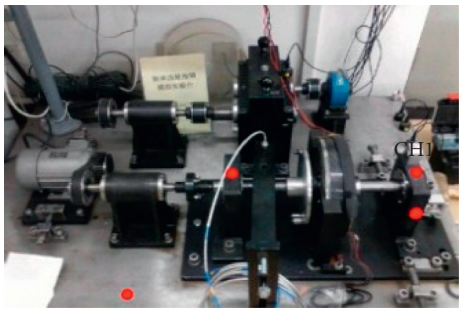

Figure 5: Fault test bench of a REB.

Table 1: The theoretical fault characteristic frequencies of different bearing parts.

BPFO	BPFI	BSF	CF
86.32	145.84	51.13	8.06

harmonic frequency, which might affect fault detection due to that BPFO is usually higher than its harmonics in most cases. In Figure 7(c), the magnitude of BPFI is higher than other frequencies except shaft rotation frequency, which is perhaps affected by the delivery path. This result may be identified as unbalanced rather than inner race fault. In Figure 7(d), the BSF is covered by CF and its harmonics, which may result in a wrong detection result.

4.2. Analysis and Comparison with Other Methods. The results of the proposed method are shown in blue lines of Figure 8. It can be seen that the proposed method is capable of reducing noise in the vibration signal.

In order to investigate the differences between the original signal and results of the proposed method, envelope demodulation is used to analyse the results. And the object of this paper is to overcome the lack of adaptability of peak-based wavelet decomposition methods. So next, we will make comparisons with the peak-based wavelet decomposition method [19].

Case I. A Point Defect on Outer Race. The results of the vibration signal induced by the outer race fault are shown in Figure 9. Figure 9(a) shows the result of envelope analysis that the magnitude of BPFO is not the remarkable one among all frequency components. And it can be seen that although the BPFO amplitude is somewhat increased in

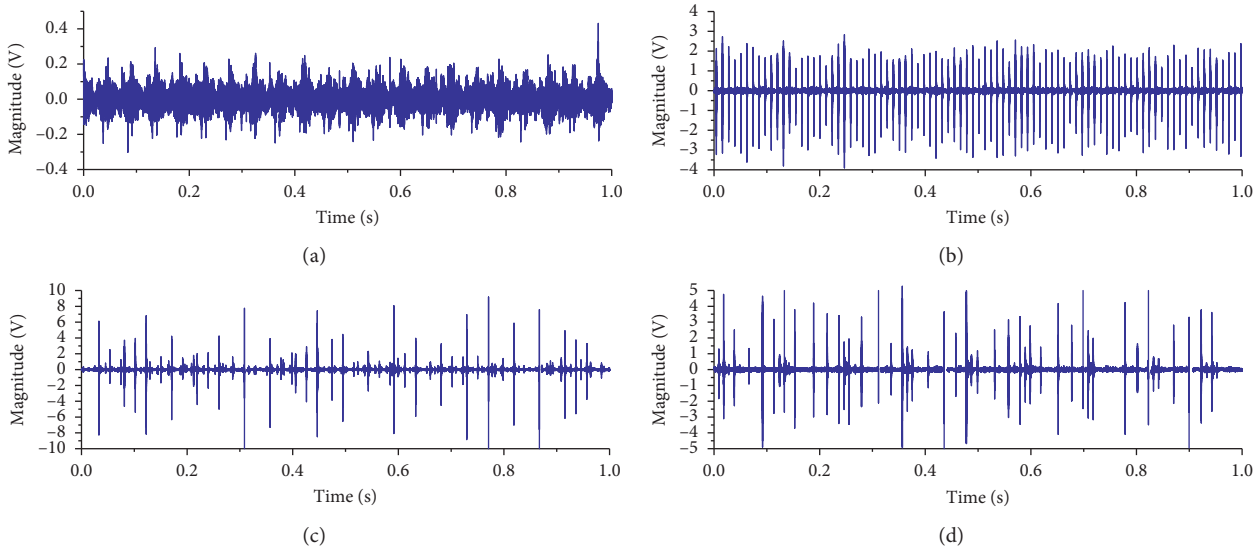

Figure 6: Vibration signals of REBs. (a) A normal REB and bearings with a point defect on (b) outer race; (c) inner race; (d) rolling element.

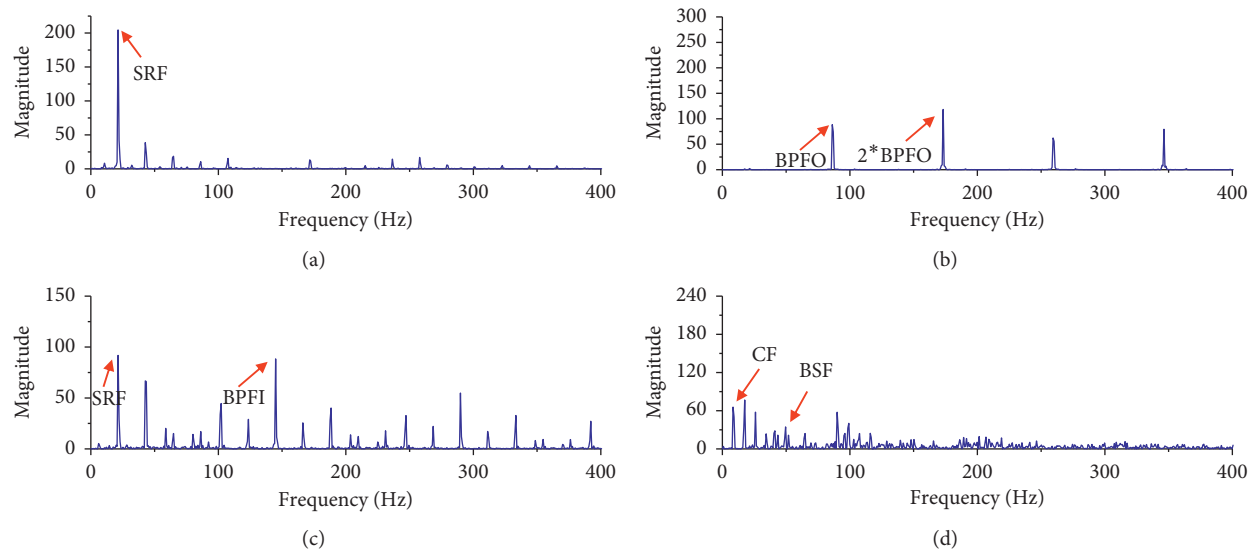

Figure 7: Envelope spectra of the vibration signal in Figure 4. (a) A normal REB and bearings with a point defect on (b) outer race; (c) inner race; (d) rolling element.

Figure 9(b), it is still not the most obvious. After parameter optimization in Figure 9(c), the magnitude of BPFO is enhanced to be the most prominent, but parameter optimization greatly increases the amount of calculation. However, it is clear that the magnitude of BPFO is enhanced to be the most outstanding one in Figure 9(d). Moreover, the proposed method is adaptive that does not require parameter optimization and the magnitude of BPFO is obviously higher than that obtained using peak-based wavelet decomposition.

Case II. A Point Defect on Inner Race. Figure 10 shows the results of the vibration signal induced by the inner race fault. It can be seen that the magnitude of SRF is the remarkable one among all frequency components in Figure 10(a) which perhaps lead to an incorrect detection result. Although BPFI has been enhanced to be the most obvious in Figure 10(b), the amplitude of SRF is close to BPFI and the result may still be interfered by SRF. In Figure 10(c), the magnitude of BPFI is the remarkable one and significantly higher than that of SRF. But the parameter optimization calculation is less efficient. Meanwhile, Figure 10(d) shows that the magnitude of BPFI is enhanced to be the most prominent and not easily interfered by SRF.

The proposed method is an adaptive method, and thus the influence of parameter optimization on the computational efficiency can be avoided. And the magnitude of BPFI with the proposed method is obviously higher than that of peak-based wavelet decomposition.

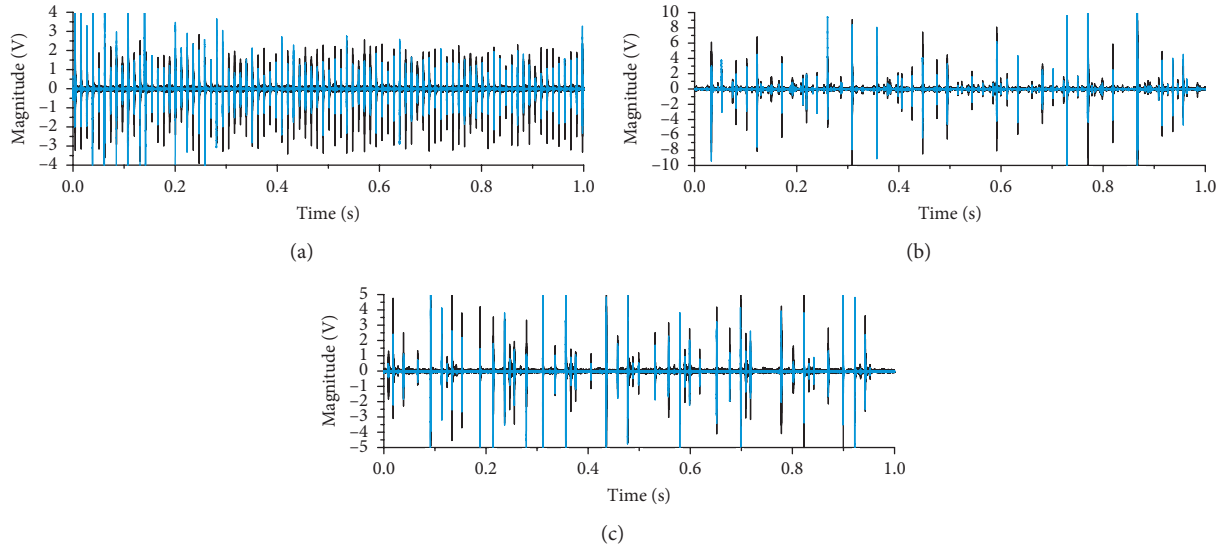

FIGURE 8: Results of the proposed method (blue line) and the original vibration signals (black line) of REBs. Bearings with a point defect on (a) outer race; (b) inner race; (c) rolling element.

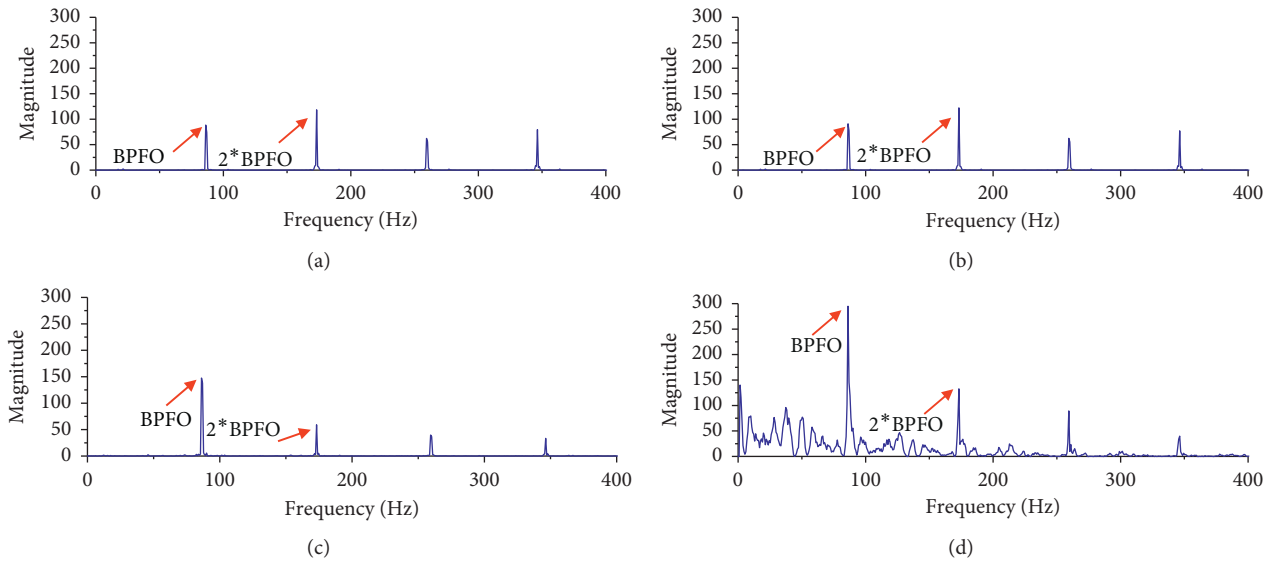

FIGURE 9: Processing result of the vibration signal induced by the outer race fault. (a) Envelope demodulation; (b) peak-based wavelet decomposition; (c) parameter-optimized peak-based wavelet decomposition; (d) proposed peak-based mode decomposition.

Case III. A Point Defect on Rolling Element. The results of the vibration signal induced by the rolling element fault are shown in Figure 11, with the envelope analysis results shown in Figure 11(a). The magnitude of BSF is covered by CF and its harmonics, so it is difficult to detect BSF through envelope analysis. Although the magnitude of BSF has increased slightly by peak-based wavelet decomposition in Figure 11(b), it is still covered by CF and its harmonics. Meanwhile, the magnitude of BSF is enhanced to be the most outstanding in Figure 11(c) which exceeds the magnitude of CF clearly. However, the parameter optimization has problems in computational efficiency. And the result of peak-based mode decomposition is shown in Figure 11(d). The magnitude of BSF is also enhanced to be the most remarkable. And the magnitude of BPFI with the proposed method is obviously higher than peak-based wavelet decomposition. In addition, the proposed method is an adaptive method which improves the efficiency of the operation.

Comparisons of some major indictors for bearing fault features are listed in Table 2. It can be seen that both peak-based wavelet decomposition and the proposed method can enhance fault frequencies. Meanwhile, the magnitude of fault frequencies with the proposed method is obviously

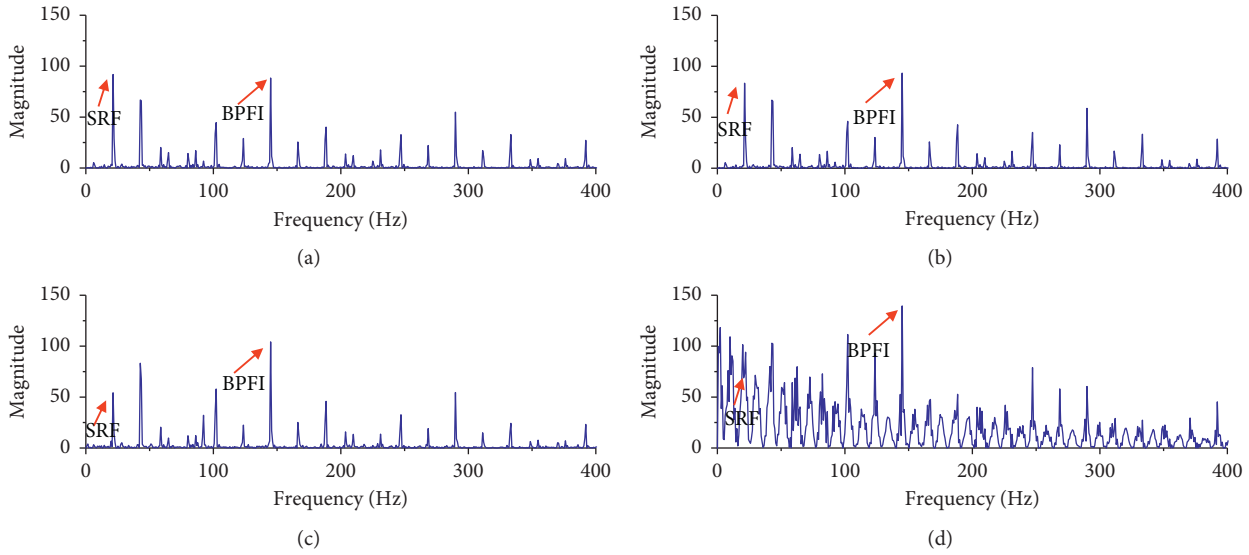

Figure 10: Processing result of the vibration signal induced by the inner race fault. (a) Envelope demodulation; (b) peak-based wavelet decomposition; (c) parameter-optimized peak-based wavelet decomposition; (d) proposed peak-based mode decomposition.

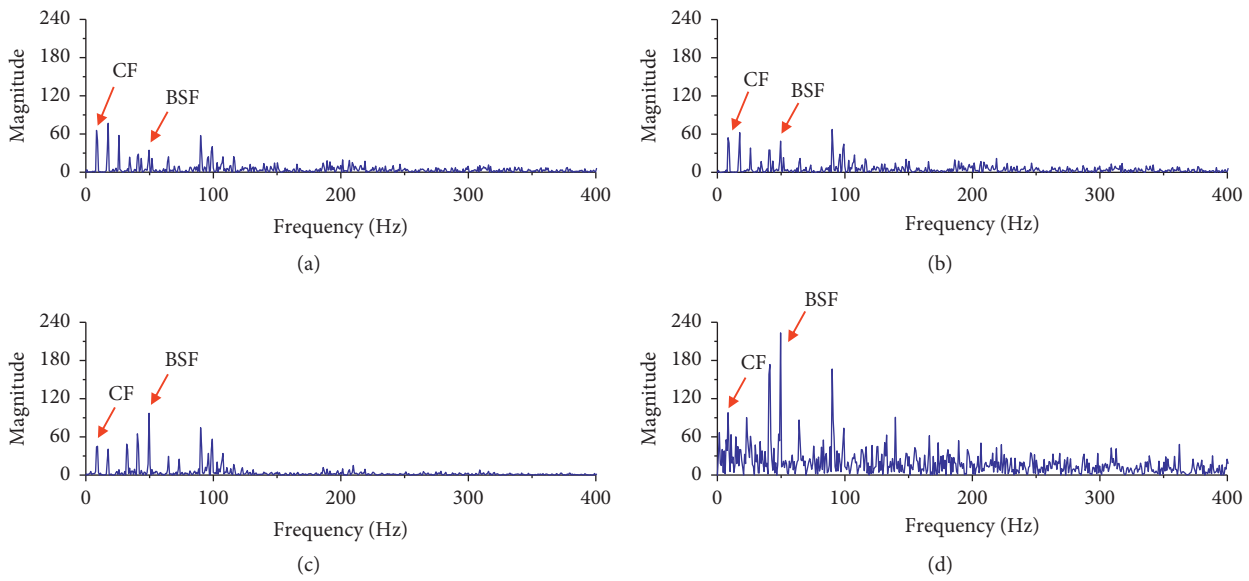

Figure 11: Processing result of the vibration signal induced by rolling element fault. (a) Envelope demodulation; (b) peak-based wavelet decomposition; (c) parameter-optimized peak-based wavelet decomposition; (d) proposed peak-based mode decomposition.

Table 2: Comparisons of some major indictors for bearing fault features.

Defect frequency magnitude of	Envelope demodulation	Peak-based wavelet decomposition	Parameter-optimized peak-based wavelet decomposition	The proposed method
Outer race	88.45	90.95	147.50	294.80
Inner race	88.40	93.34	104.20	139.50
Roller element	34.56	48.96	97.08	223.30

higher than the other methods. Because the amplitude of the squared envelope spectrum is normalized, the larger the amplitude of the characteristic frequency of the fault, the more it deviates from the normal state and the more likely it is abnormal. In other words, signals processed by the proposed method become easier to be detected. Moreover, the proposed method is an adaptive method, which does not need to optimize parameters.

5. Conclusions

In order to overcome the lack of adaptability of peak-based wavelet decomposition, the present paper proposed peak-based mode decomposition for bearing fault diagnosis. The proposed method can eliminate noise adaptively in a vibration signal and enhance and well-detect the weak repetitive transients. Simulation and experiments verify the effectiveness of the proposed method. Compared with the peak-based wavelet decomposition, the proposed method not only can enhance the fault characteristics more significantly, but also is an adaptive algorithm, which does not need to optimize parameters such as the base functions and thresholds.

Data Availability

The data used to support the findings of this study are available from the corresponding author upon request.

Conflicts of Interest

The authors declare that there are no conflicts of interest regarding the publication of this paper.

Acknowledgments

This work was partially supported by the Open Fund of State Key Laboratory of Nuclear Power Safety Monitoring Technology and Equipment, Shenzhen, Guangdong, 518172, China (Grant no. K-A2018.426).

References

[1] G. Tang, Q. Yang, H.-Q. Wang, G.-G. Luo, and J.-W. Ma, "Sparse classification of rotating machinery faults based on compressive sensing strategy," *Mechatronics*, vol. 31, pp. 60–67, 2015.

[2] D. Yu, J. Cheng, and Y. Yang, "Application of EMD method and Hilbert spectrum to the fault diagnosis of roller bearings," *Mechanical Systems and Signal Processing*, vol. 19, no. 2, pp. 259–270, 2005.

[3] Y. Zhang, Y. Zhou, G. Tang, and H. Wang, "Multivariable least squares support vector machine with time integral operator for the prediction of bearing performance degradation," *Proceedings of the Institution of Mechanical Engineers, Part C: Journal of Mechanical Engineering Science*, vol. 233, no. 7, pp. 2478–2490, 2019.

[4] M. Khazaee, A. Rezaniakolaie, A. Moosavian, and L. Rosendahl, "A novel method for autonomous remote condition monitoring of rotating machines using piezoelectric energy harvesting approach," *Sensors & Actuators: A. Physical*, vol. 295, pp. 37–50, 2019.

[5] A. Jeanes, P. G. Coen, N. S. Drey, and D. J. Gould, "Moving beyond hand hygiene monitoring as a marker of infection prevention performance: development of a tailored infection control continuous quality improvement tool," *AJIC: American Journal of Infection Control*, vol. 48, no. 1, pp. 68–76, 2019.

[6] J. Antoni and R. B. Randall, "A stochastic model for simulation and diagnostics of rolling element bearings with localized faults," *Journal of Vibration and Acoustics*, vol. 125, no. 3, pp. 282–289, 2003.

[7] R. B. Randall, J. Antoni, and S. Chobsaard, "The relationship between spectral correlation and envelope analysis in the diagnostics of bearing faults and other cyclostationary machine signals," *Mechanical Systems and Signal Processing*, vol. 15, no. 5, pp. 945–962, 2001.

[8] D. Ho and R. B. Randall, "Optimisation of bearing diagnostic techniques using simulated and actual bearing fault signals," *Mechanical Systems and Signal Processing*, vol. 14, no. 5, pp. 763–788, 2000.

[9] D. Abboud, M. Elbadaoui, W. A Smith, and R. B. Randall, "Advanced bearing diagnostics: a comparative study of two powerful approaches," *Mechanical Systems and Signal Processing*, vol. 114, pp. 604–627, 2019.

[10] G. Tang, Y. Wang, Y. Huang, N. Liu, and J. He, "Compound bearing fault detection under varying speed conditions with virtual multi-channel signals in angle domain," *IEEE Transactions on Instrumentation and Measurement*, 2020.

[11] L. Li, Y. Cui, R. Chen, and X. Liu, "Optimal SES selection based on SVD and its application to incipient bearing fault diagnosis," *Shock and Vibration*, vol. 2018, pp. 1–13, 2018.

[12] H. Qiu, J. Lee, J. Lin, and G. Yu, "Wavelet filter-based weak signature detection method and its application on rolling element bearing prognostics," *Journal of Sound and Vibration*, vol. 289, no. 4-5, pp. 1066–1090, 2006.

[13] G. Li, G. Tang, G. Luo, and H. Wang, "Underdetermined blind separation of bearing faults in hyperplane space with variational mode decomposition," *Mechanical Systems and Signal Processing*, vol. 120, pp. 83–97, 2019.

[14] R. Yan, R. X. Gao, and X. Chen, "Wavelets for fault diagnosis of rotary machines: a review with applications," *Signal Processing*, vol. 96, pp. 1–15, 2014.

[15] K. Zhu, W. Y. San, and G. S. Hong, "Wavelet analysis of sensor signals for tool condition monitoring: a review and some new results," *International Journal of Machine Tools and Manufacture*, vol. 49, no. 7-8, pp. 537–553, 2009.

[16] R. Kumar and M. Singh, "Outer race defect width measurement in taper roller bearing using discrete wavelet transform of vibration signal," *Measurement*, vol. 46, no. 1, pp. 537–545, 2013.

[17] C. Mishra, A. K. Samantaray, and G. Chakraborty, "Rolling element bearing fault diagnosis under slow speed operation using wavelet de-noising," *Measurement*, vol. 103, pp. 77–86, 2017.

[18] P. Du, W. A. Kibbe, and S. M. Lin, "Improved peak detection in mass spectrum by incorporating continuous wavelet transform-based pattern matching," *Bioinformatics*, vol. 22, no. 17, pp. 2059–2065, 2006.

[19] H. Q. Wang, W. Hou, G. Tang, H. Yuan, Q. Zhao, and X. Cao, "Fault detection enhancement in rolling element bearings via peak-based multiscale decomposition and envelope demodulation," *Mathematical Problems in Engineering*, vol. 2014, Article ID 329458, 11 pages, 2014.

[20] Y. Lei, J. Lin, Z. He, and M. Zuo, "A review on empirical mode decomposition in fault diagnosis of rotating machinery," *Mechanical Systems and Signal Processing*, vol. 35, no. 1-2, pp. 108–126, 2013.

[21] Z. He, "Peak transform for efficient image representation and coding," *IEEE Transactions on Image Processing*, vol. 16, no. 7, pp. 1741–1754, 2007.

[22] N. E. Huang, Z. Shen, S. R. Long et al., "The empirical mode decomposition and the Hilbert spectrum for nonlinear and non-stationary time series analysis," *Proceedings of the Royal*

Society of London. Series A: Mathematical, Physical and Engineering Sciences, vol. 454, no. 1971, pp. 903–995, 1998.

[23] J. Antoni, F. Bonnardot, A. Raad, and M. El Badaoui, "Cyclostationary modelling of rotating machine vibration signals," *Mechanical Systems and Signal Processing*, vol. 18, no. 6, pp. 1285–1314, 2004.